Design analysis of doped-silicon surface plasmon resonance immunosensors in mid-infrared range

William DiPippo,[1] Bong Jae Lee,[2] and Keunhan Park[1,*]

[1] *Department of Mechanical, Industrial and Systems Engineering, University of Rhode Island, Kingston, RI 02881 USA*
[2] *Department of Mechanical Engineering and Material Science, University of Pittsburgh, Pittsburgh, PA 15261 USA*
**kpark@egr.uri.edu*

Abstract: This paper reports the design analysis of a microfabricatable mid-infrared (mid-IR) surface plasmon resonance (SPR) sensor platform. The proposed platform has periodic heavily doped profiles implanted into intrinsic silicon and a thin gold layer deposited on top, making a physically flat grating SPR coupler. A rigorous coupled-wave analysis was conducted to prove the design feasibility, characterize the sensor's performance, and determine geometric parameters of the heavily doped profiles. Finite element analysis (FEA) was also employed to compute the electromagnetic field distributions at the plasmon resonance. Obtained results reveal that the proposed structure can excite the SPR on the normal incidence of mid-IR light, resulting in a large probing depth that will facilitate the study of larger analytes. Furthermore, the whole structure can be microfabricated with well-established batch protocols, providing tunability in the SPR excitation wavelength for specific biosensing needs with a low manufacturing cost. When the SPR sensor is to be used in a Fourier-transform infrared (FTIR) spectroscopy platform, its detection sensitivity and limit of detection are estimated to be 3022 nm/RIU and ~70 pg/mm^2, respectively, at a sample layer thickness of 100 nm. The design analysis performed in the present study will allow the fabrication of a tunable, disposable mid-IR SPR sensor that combines advantages of conventional prism and metallic grating SPR sensors.

OCIS codes: (130.3060) Infrared; (130.6010) Sensors; (220.4000) Microstructure fabrication; (230.1950) Diffraction gratings; (240.6680) Surface plasmons.

References and links

1. H. Raether, *Surface Plasmons on Smooth and Rough Surfaces and on Gratings* (Springer, 1988).
2. J. Homola, "Present and future of surface plasmon resonance biosensors," Anal. Bioanal. Chem. **377**(3), 528–539 (2003).
3. C. Y. Yang, E. Brooks, Y. Li, P. Denny, C. M. Ho, F. Qi, W. Shi, L. Wolinsky, B. Wu, D. T. W. Wong, and C. D. Montemagno, "Detection of picomolar levels of interleukin-8 in human saliva by SPR," Lab Chip **5**(10), 1017–1023 (2005).
4. E. Suraniti, E. Sollier, R. Calemczuk, T. Livache, P. N. Marche, M. B. Villiers, and Y. Roupioz, "Real-time detection of lymphocytes binding on an antibody chip using SPR imaging," Lab Chip **7**(9), 1206–1208 (2007).
5. K. S. Phillips, and Q. Cheng, "Recent advances in surface plasmon resonance based techniques for bioanalysis," Anal. Bioanal. Chem. **387**(5), 1831–1840 (2007).
6. X. D. Hoa, A. G. Kirk, and M. Tabrizian, "Towards integrated and sensitive surface plasmon resonance biosensors: a review of recent progress," Biosens. Bioelectron. **23**(2), 151–160 (2007).
7. K. Johansen, H. Arwin, I. Lundstrom, and B. Liedberg, "Imaging surface plasmon resonance sensor based on multiple wavelengths: Sensitivity considerations," Rev. Sci. Instrum. **71**(9), 3530–3538 (2000).
8. are S. Patskovsky, A. V. Kabashin, M. Meunier, and J. H. T. Luong, "Properties and sensing characteristics of surface-plasmon resonance in infrared light," J. Opt. Soc. Am. A **20**(8), 1644–1650 (2003).
9. R. Ziblat, V. Lirtsman, D. Davidov, and B. Aroeti, "Infrared surface plasmon resonance: a novel tool for real time sensing of variations in living cells," Biophys. J. **90**(7), 2592–2599 (2006).
10. Y. B. Chen, "Development of mid-infrared surface plasmon resonance-based sensors with highly-doped silicon for biomedical and chemical applications," Opt. Express **17**(5), 3130–3140 (2009).

#130418 - $15.00 USD Received 24 Jun 2010; revised 7 Aug 2010; accepted 10 Aug 2010; published 27 Aug 2010

11. J. Homola, S. Yee, and G. Gauglitz, "Surface Plasmon Resonance Sensors: Review," Sens. Actuators B Chem. **54**(1-2), 3–15 (1999).
12. M. Piliarik, H. Vaisocherová, and J. Homola, "Surface plasmon resonance biosensing," Methods Mol. Biol. **503**, 65–88 (2009).
13. S. Basu, B. Lee, and Z. Zhang, "Infrared Radiative Properties of Heavily Doped Silicon at Room Temperature," J. Heat Transfer **132**(2), 023301 (2010).
14. J. G. Huang, C. L. Lee, H. M. Lin, T. L. Chuang, W. S. Wang, R. H. Juang, C. H. Wang, C. K. Lee, S. M. Lin, and C. W. Lin, "A miniaturized germanium-doped silicon dioxide-based surface plasmon resonance waveguide sensor for immunoassay detection," Biosens. Bioelectron. **22**(4), 519–525 (2006).
15. H. Sai, H. Yugami, Y. Akiyama, Y. Kanamori, and K. Hane, "Spectral control of thermal emission by periodic microstructured surfaces in the near-infrared region," J. Opt. Soc. Am. A **18**(7), 1471–1476 (2001).
16. M. Laroche, F. Marquier, R. Carminati, and J. Greffet, "Tailoring Silicon Radiative Properties," Opt. Commun. **250**(4-6), 316–320 (2005).
17. B. Lee, Y. Chen, and Z. Zhang, "Transmission Enhancement Through Nanoscale Metallic Slit Arrays from the Visible to Mid-Infrared," J. Comput. Theo. Nano. **5**, 201–213 (2008).
18. M. Moharam, E. Grann, D. Pommet, and T. Gaylord, "Formulation for Stable and Efficient Implementation of the Rigorous Coupled-Wave Analysis of Binary Gratings," J. Opt. Soc. Am. A **12**(5), 1068–1076 (1995).
19. M. Moharam, and T. Gaylord, "Rigorous Coupled-Wave Analysis of Planar-Grating Diffraction," J. Opt. Soc. Am. **71**(7), 811–818 (1981).
20. W. Lee, and F. Degertekin, "Rigorous Coupled-Wave Analysis of Multilayered Grating Structures," J. Lightwave Technol. **22**(10), 2359–2363 (2004).
21. K. Byun, S. Kim, and D. Kim, "Design study of highly sensitive nanowire-enhanced surface plasmon resonance biosensors using rigorous coupled wave analysis," Opt. Express **13**(10), 3737–3742 (2005).
22. D. Zhang, P. Wang, X. Jiao, G. Yuan, J. Zhang, C. Chen, H. Ming, and R. Rao, "Investigation of the Sensitivity of H-Shaped Nano-Grating Surface Plasmon Resonance Biosensors Using Rigorous Coupled Wave Analysis," Appl. Phys. Lett. A **89**(2), 407–411 (2007).
23. B. Wu, and Q. Wang, "High Sensitivity Transmission-Type SPR Sensor by using Metallic-Dielectric Mixed Gratings," Chin. Phys. Lett. **25**(5), 1668–1671 (2008).
24. B. Lee, Y. Chen, and Z. Zhang, "Confinement of Infrared Radiation to Nanometer Scales Through Metallic Slit Arrays," J. Quant. Spectrosc. Radiat. Transf. **109**(4), 608–619 (2008).
25. J. Jin, *The Finite Element Method in Electromagnetics* (Wiley-IEEE Press, 2002).
26. E. D. Palik, *Handbook of Optical Constants of Solids II* (Academic Press, 1991).
27. F. Marquier, K. Joulain, J. Mulet, R. Carminati, J. Greffet, and Y. Chen, "Coherent Spontaneous Emission of Light by Thermal Sources," Phys. Rev. B **69**(15), 155412 (2004).
28. J. J. Greffet, R. Carminati, K. Joulain, J. P. Mulet, S. Mainguy, and Y. Chen, "Coherent emission of light by thermal sources," Nature **416**(6876), 61–64 (2002).
29. K. Park, B. Lee, C. Fu, and Z. Zhang, "Study of the surface and bulk polaritons with a negative index metamaterial," J. Opt. Soc. Am. B **22**(5), 1016–1023 (2005).
30. J. De Feijter, J. Benjamins, and F. Veer, "Ellipsometry as a Tool to Study the Adsorption Behavior of Synthetic and Biopolymers at the Air-Water Interface," Biopolymers **17**, 3530–3538 (2000).
31. T. Tumolo, L. Angnes, and M. S. Baptista, "Determination of the refractive index increment (dn/dc) of molecule and macromolecule solutions by surface plasmon resonance," Anal. Biochem. **333**(2), 273–279 (2004).
32. S. J. Chen, F. C. Chien, G. Y. Lin, and K. C. Lee, "Enhancement of the resolution of surface plasmon resonance biosensors by control of the size and distribution of nanoparticles," Opt. Lett. **29**(12), 1390–1392 (2004).

1. Introduction

A surface plasmon is a localized electromagnetic (EM) wave that propagates along the metal-dielectric interface and exponentially decays into both media [1]. Surface plasmons can be excited due to the resonant transfer of the incident photon energy and momentum to collectively oscillate electrons in a noble metal, resulting in a sharp dip in the reflectance spectrum. Hence, the excitation of surface plasmons is called the surface plasmon resonance (SPR). Since the SPR is the resonance phenomenon, its excitation condition is extremely sensitive to the refractive index of the adjacent medium near the interface. For example, when biomolecular recognition elements at the metal surface selectively capture analytes in a liquid sample, the reflectance dip makes a shift due to the change of local refractive index near the surface. This characteristics promises the application of the SPR for lab-on-chip immunosensors [2]: accurate measurement of the reflectance shift and its correlation with the binding-induced refractive index change allows the label-free detection of biological analytes to the unprecedented sensitivity of picomolar level [3]. Furthermore, even real-time monitoring of biomolecular interaction is possible owing to the fast measurement scheme by optical means [4].

While remarkable progress has been made in developing SPR-based instrumentations for monitoring in real time the interactions between various biomolecules [2,5,6], most research

#130418 - $15.00 USD Received 24 Jun 2010; revised 7 Aug 2010; accepted 10 Aug 2010; published 27 Aug 2010

has focused on the visible wavelength range owing to the relatively simple yet accurate instrumentation with visible-range laser sources. However, SPR detection in the mid-IR range (1 μm < λ < 11 μm) provides several beneficial effects over that in the visible range. First, the use of a longer wavelength as a light source excites surface plasmons that have a larger penetration depth into a sample side [7] and experience less scattering during propagation along the interface [8], which will allow the accurate detection of the SPR dip position for larger samples, such as living cells [2]. Another advantage is that most biological specimens are practically transparent upon exposure to mid-IR radiation. Thus, in contrast to the photodamage potentially induced by the visible-range radiation, the mid-IR light would not cause photodamage or phototoxicity to biosamples [9]. However, conventional SPR sensor platforms, such as a metal-coated prism or a metallic grating, have some challenges to be directly used in the mid-IR range, mainly due to manufacturing and instrumentation costs. Moreover, a grating structure may cause nonspecific binding of analytes in its periodic groves [10], as metallic gratings do not offer a physically flat surface for the easy surface functionalization of biomolecular recognition elements (BRE), such as antibodies, antigens, affibodies, peptides, oligonucleotides or molecular imprinted polymers [11,12]. Recently, Chen [10] proposed a mid-IR SPR sensor that has a periodic undoped profile embedded in a heavily doped substrate, demonstrating that his sensor is optically analogous to a metallic grating coupler and can excite the SPR. While Ref [10]. is the first work that suggests the doped-Si grating structure as a biosensor, challenges may arise during its fabrication, particularly when uniformly doping substrate while periodic grating regions remain undoped. Another challenging issue is that the heavily doped substrate only allows the beam incidence from the topside where culture fluid exists, which may cause significant IR absorption due to water molecules. Thus the key to resolve these imposing challenges would be to develop a mid-IR SPR coupler that provides a flat surface for the best specific binding environments while being cost-effective in its manufacturing, maintenance and instrumentation.

This paper reports the design analysis of a mid-IR SPR sensor that resolves the aforementioned issues of current SPR platforms and can be fabricated using readily available mircoelectromechanical system (MEMS) processes. Figure 1 illustrates the schematic diagram

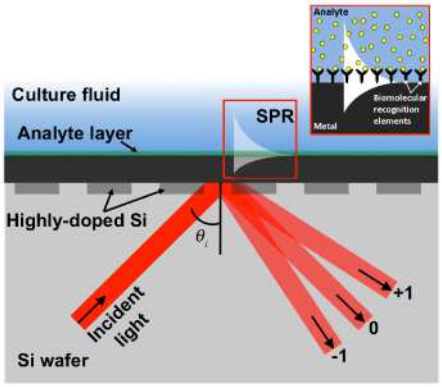

Fig. 1. Schematic of the doped-Si SPR biosensor platform (not scaled). The silicon diffraction grating couples the incident light to resonate surface charge density oscillations at the metal-analyte interface. The excited surface plasmon probes surface composition changes as a result of binding events between analyte and functionalized biomolecular recognition elements.

of the proposed SPR platform, where a heavily doped profile is periodically implanted in an intrinsic silicon wafer and a thin gold layer is deposited on top. Notice that optical characteristics of silicon, which is intrinsically transparent in the IR region (i.e., λ > 1.1 μm), becomes metallic when heavily doped [13]. Therefore, the embedded heavily doped profile will play a role as a diffraction grating although the substrate is flat and can excite a surface

#130418 - $15.00 USD Received 24 Jun 2010; revised 7 Aug 2010; accepted 10 Aug 2010; published 27 Aug 2010

plasmon on the gold-sample interface. In fact, tunable optical properties of silicon using a doping-level control have been applied in various sensors [10,14] and thermal emitters [15,16]. In order to theoretically demonstrate the feasibility of the proposed SPR coupler, rigorous coupled wave analysis (RCWA) [17,18] and finite element analysis (FEA) schemes will be used to compute the reflectance spectrum in the mid-IR region and the corresponding electromagnetic (EM) field distribution in vicinity of the coupler. The performance analysis is also conducted when the proposed sensor is integrated with the Fourier transform infrared (FTIR) spectroscopy, which would significantly reduce the instrumentation cost.

2. Modeling

In the present study, the RCWA algorithm was used to calculate the directional-hemispherical reflectance of the silicon diffraction grating. Owing to its effectiveness in solving Maxwell's equations, RCWA has been used extensively for the analysis of radiative properties of grooved surfaces [19,20] along with some recent works in studying the sensitivity of various SPR couplers [21–23]. In the RCWA algorithm, the electric and magnetic fields in the incident, grating, and transmitted media are expanded as a summation of multiple diffraction orders. Due to the periodicity of the grating structure, the dielectric function (or relative electric permittivity) of the grating region can be expressed as a Fourier expansion. By matching the boundary conditions (i.e., continuity of tangential components of electric and magnetic fields) at boundaries of the incident, grating, and transmitted media, closed linear equations can be obtained. By following previous studies [17,24], a total of 81 Fourier components are used to represent the dielectric function in the grating region, and the results differ from those obtained with 201 terms by less than 0.3%. Notice that the geometry of gratings is defined by the period (Λ), thickness (d), and the width (w) of the heavily doped strip. Hence, the filling ratio of heavily doped Si is given by $f = 1-w/\Lambda$. In the designing process to optimize the geometric parameters, the RCWA was employed due to its relatively faster computation time. For instance, at a given wavelength and geometric parameters, the calculation of the reflectance using RCWA algorithm takes about 0.12 s of CPU time with an Intel Core2 Quad Processor.

A finite element analysis (FEA) using COMSOL Multiphysics software was also used to compute the EM field distribution when a surface plasmon is excited. For the computation, the system was 2-D modeled over a 20 μm × 40 μm area. This area encompassed 10 periods of the diffraction grating and was found to be sufficiently large such that boundary effects do not alter EM field distribution. The harmonic propagation of a transverse magnetic (TM)-plane wave was incident upon the diffraction grating composed of several domains all of which have wavelength-dependent refractive indices. Mesh creation within these domains was precisely controlled such that the maximum spacing between each calculation node, Δ_{max}, satisfies the relation $\Delta_{max} = \lambda / 8n$ where λ is the wavelength of incident radiation and n is the local refractive index. The eight calculation points per wavelength ensure the convergence of the EM field computation [25]. Intermediate calculation sites due to the higher-order quadratic elements used in the triangular mesh generation further improve the accuracy of the numeric method. Over 390,000 degrees of freedom were solved with an Intel Core2 Quad Processor, resulting in a calculation time of approximately 16 seconds of CPU time. The FEA analysis was only completed once the finalized geometric parameters were determined via RCWA.

The structure used in the numerical analysis consisted of a silicon diffraction grating with a 4-μm period and a filling ratio of 0.5. Uniform gratings of 800 nm in depth into the bulk intrinsic silicon are phosphorous-doped at a concentration of 10^{20} cm^{-3}. This doping concentration, as previously mentioned, is high enough to show metallic behaviors to the IR radiation while the bulk intrinsic silicon remains transparent to incident wavelengths greater than 1.1 μm. An 8-nm gold layer is deposited on the silicon structure providing a medium that supports surface plasmons and BRE attachment. Optical properties of heavily doped Si are calculated using Drude models [13]. Notice that both the plasma frequency and damping terms for doped Si are dependent on carrier concentration, which can be managed via implant

#130418 - $15.00 USD Received 24 Jun 2010; revised 7 Aug 2010; accepted 10 Aug 2010; published 27 Aug 2010

dosage. In the analysis, water was used as a culture fluid. The water absorption was considered in the calculation. The optical properties of water and Au were all obtained by an interpolation of tabulated data in Ref [26]. For simplicity of the calculation, the Si substrate was assumed to be semi-infinite and lossless.

3. Results and discussion

In order to demonstrate the feasibility of the doped-Si SPR coupler, Fig. 2(a) shows the dispersion relation of the SPR excitation through the modulation of both vacuum wavelength and incidence angle, and Fig. 2(b) shows the reflectance spectrum for different incidence angles. Sharp dips observed in the reflectance indicate that the SPR coupler excites two SPRs at the oblique incidence, but the strongest SPR is excited at the normal incidence. The excitation of two SPRs at the oblique incidence is because the dispersion curves are fold back to the reduced zone of $0 \le k_x \le \pi/\Lambda$, where k_x is the wavevector component parallel to the interface, due to the periodicity (or discrete translational symmetry) [27]. However, multiple SPR excitations in grating structures predicted in literature [10,28] are not observed in the considered structure except at the fundamental SPR condition. We believe that the higher order diffractions, which are responsible for multiple SPR excitations, are too weak to induce sharp reflectance dips in our configuration. The strongest SPR at the normal incidence supports the integration of an IR microscope to focus the IR light onto the microscale SPR platform, promising for the microfabrication of a SPR sensor array for multi-assay screening [4].

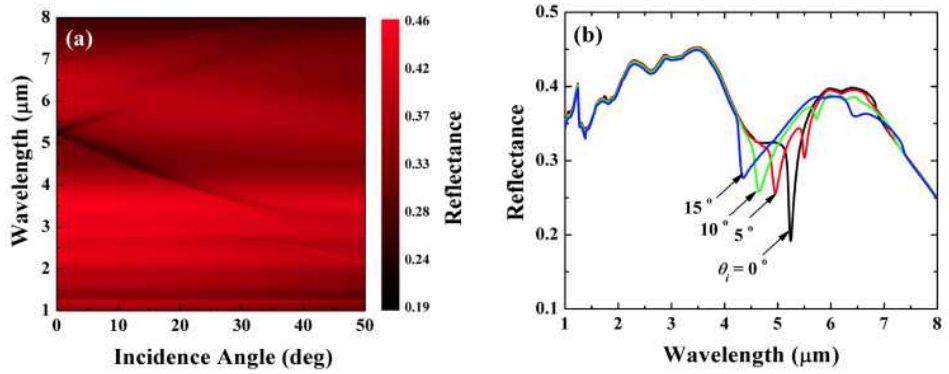

Fig. 2. (a) Dispersion relation of the doped-Si SPR coupler. Due to the grating harmonics of the doped silicon regions, SPR is observed at a wavelength of 5.24 μm for the normal incidence of IR light. Two coupling points are observed at oblique incidence angles due to the periodicity of the grating structure. (b) Reflectance curves demonstrate normal incidence provides the best sharpness as compared to oblique setups.

Figure 3 compares the normalized magnitude of electric field distributions at (a) 4 μm, (b) 5.24 μm, and (c) 9 μm, where SPR is excited at λ_{sp} = 5.24 μm for the given geometry. At the surface plasmon wavelength λ_{sp}, an exponentially decaying EM field into both the gold and dielectric layers propagates along the interface. It should be noted that the gold layer should be sufficiently thin as compared to its skin depth in order for diffracted wave to evanescently tunnel through the metal film and excite a surface plasmon at the upper boundary. As shown in Fig. 3(b), the surface plasmon wave exhibits a large penetration depth of 3.9 μm in the dielectric medium and thus will allow the detection of comparatively thick samples while maintaining a high sensitivity for the detection of small concentrations of analyte. At other wavelengths, free electrons within gold indiscriminately oscillate out of phase with the incident light; thus, reflecting incident light back to the Si substrate and preventing resonant photon-electron energy transfer. The incident IR light is predominantly reflected by the gold layer due to its high reflectance at both Figs. 3(a) and 3(c), whilst at shorter wavelength a small portion of light is transmitted through the thin gold layer.

#130418 - $15.00 USD Received 24 Jun 2010; revised 7 Aug 2010; accepted 10 Aug 2010; published 27 Aug 2010

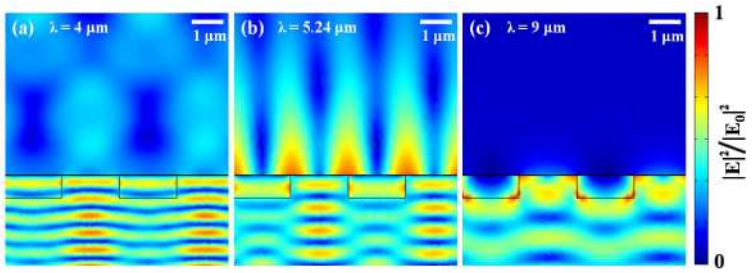

Fig. 3. FEA simulation displaying the normalized electric field magnitude in vicinity of the designed sensor for incident wavelengths of: (a) 4 μm, (b) 5.24 μm, and (c) 9 μm. At the SPR wavelength, (b), a standing surface wave is formed at the metal-dielectric interface which evanescently penetrates the dielectric medium to a skin depth of 3.9 μm. At other wavelengths, the incident IR light is predominantly reflected by the gold layer due to its high reflectance, while a small portion of light is transmitted through the thin gold layer at shorter wavelengths.

The proposed SPR platform offers a high tunability in plasmon resonance position. A diffraction grating adds additional wave momentum required to match that of the SPR surface wave by a factor $\pm j2\pi/\Lambda$, where j is the diffraction order [10]. Thus, a large range in wavelengths can be used to excite a surface plasmon simply by adjusting the grating period. This concept is proved in Fig. 4 by changing the grating period while other parameters (i.e., grating thickness and doping concentration, gold layer thickness, and the filling ratio) remain the same as the design. As shown in Fig. 4(a), a small change of the grating period shifts the reflectance dip position with a slight change of the dip width and depth. The grating period is linearly proportional the shift of the dip position over a large range of wavelength, e.g., from 3 μm to 9 μm in Fig. 4(b). It should be noted that the dip position could be further shifted beyond what is shown in Fig. 4(b). This tunability of the SPR excitation suggests that the SPR wavelength can be precisely tailored depending on sizes and characteristics of analytes. For example, relatively small analytes may need a small penetration depth, thus short-wavelength SPRs for better sensitivity while those demanding a large penetration depth can be accurately studied using larger wavelengths. Moreover, when IR laser sources are to be used with the sensor, the SPR wavelength can be tuned to that of a laser source for the optimal performance.

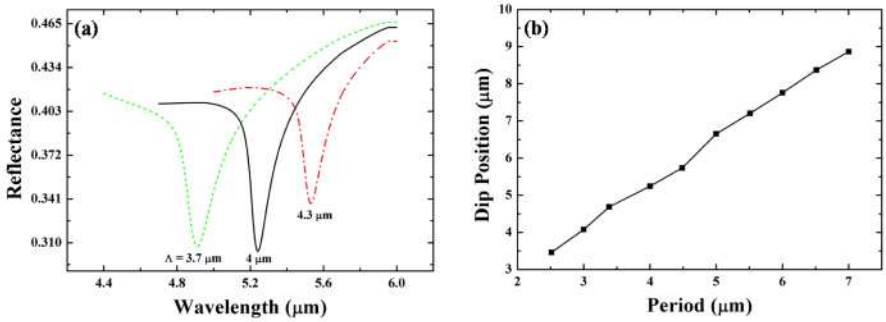

Fig. 4. Proposed coupler offers ease in tuning SPR wavelength. (a) Examples of reflectance dip position shifts as a result of grating period change. Thus, the linear shift observed in (b) enables plasmon excitation at ends of the IR-spectrum through simple manipulation of implant trench periodicity.

#130418 - $15.00 USD Received 24 Jun 2010; revised 7 Aug 2010; accepted 10 Aug 2010; published 27 Aug 2010

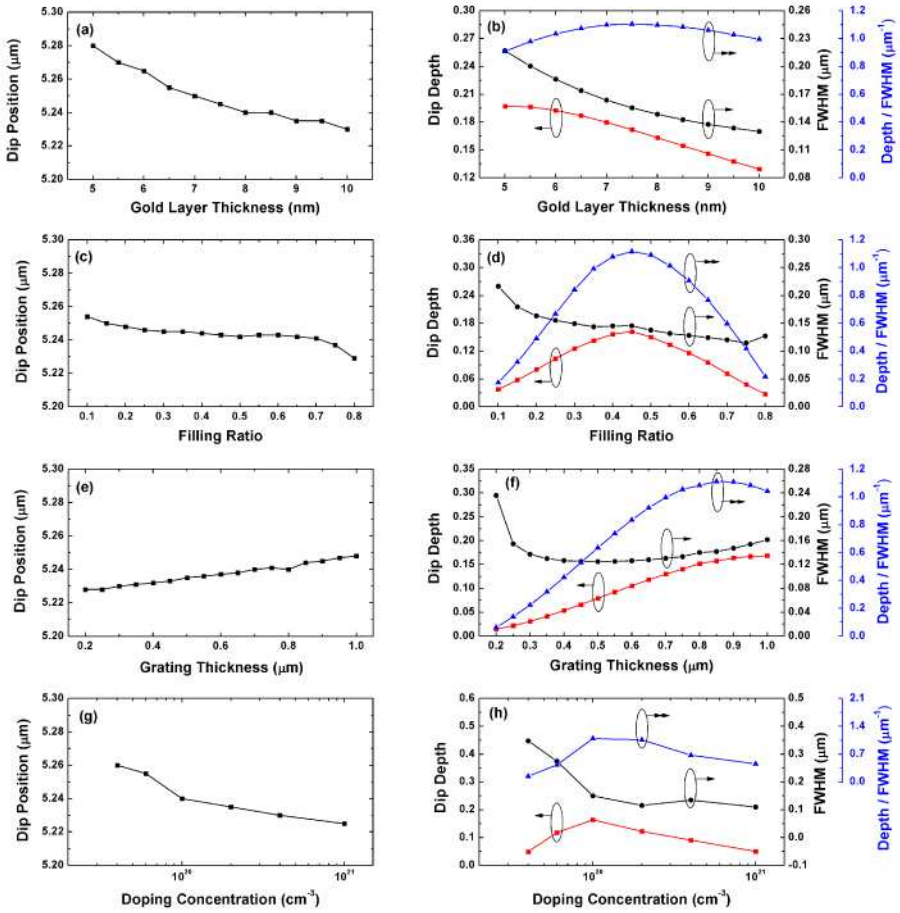

Fig. 5. RCWA-based parametric study on the SPR excitation. A small change in dip position is seen for increasing (a) gold layer thickness, (c) filling ratio, (e) grating thickness, and (g) doping concentration. The reflectance dip depth and FWHM also change for adjustment in (b) gold layer thickness, (d) filling ratio, (f) grating thickness, and (h) doping concentration.

The effects of remaining design parameters (i.e., gold layer thickness, filling ratio, grating thickness, and doping concentration) on the SPR excitation are shown in Fig. 5. This parametric study was performed by changing one parameter while the others remain as design values, i.e., 4 μm for the grating period, 8 nm for the gold layer thickness, 0.5 for the filling ratio, 800 nm for the grating depth, and 10^{20} cm^{-3} for the doping concentration. When compared to Fig. 4, these parameters do not demonstrate a substantial impact on the SPR position as the grating period; the change is less than 1% for all parameters. The dip position shifts caused by changing the gold layer and the grating thicknesses are likely due to the weak coupling of forward and backward evanescent waves in the gold layer [29]. The filling ratio has a negligible effect on the dip position except the extreme cases. Dip position shift resulting from the doping concentration is likely due to the alteration of optical properties of the grating. As shown in Fig. 5(b), the gold layer thickness also modifies the dip quality – the dip depth and the full-width at half minimum (FWHM). In order to qualitatively describe the dip sharpness, the ratio of the dip depth to the FWHM is also shown in the plot; the increase of this ratio indicates a sharper dip. Increasing the thickness of the gold layer reduces the dip depth, indicating the excitation of a weaker SPR due to the attenuation of the diffracted evanescent wave to the gold-medium interface. The reduction of the FWHM with the increase

#130418 - $15.00 USD Received 24 Jun 2010; revised 7 Aug 2010; accepted 10 Aug 2010; published 27 Aug 2010

of the gold layer thickness can be explained with the decrease of radiative losses due to weaker forward-backward wave coupling [29]. Consequently, the best sharpness can be found at between 7 nm and 8 nm of the gold layer. Figure 5(d) clearly shows the effect of the filling ratio on the dip quality, which provides the best for the filling ratio of 0.45. In Fig. 5(f), the thicker gratings cause the deeper reflectance dip. However, the sharpness is not necessarily proportional to the grating thickness, as the thicker gratings may cause more scattering during the propagation of surface plasmons and increases the dip width. The optimal grating thickness for a 4-μm period structure is approximately 800 nm. The effect of the doping concentration on the dip quality shown in Fig. 5(h) provides a counterintuitive result that although a heavily doped Si becomes more metallic, a heavily-doped Si grating does not excite a better SPR. The optimal doping concentration for the proposed sensor is around 10^{20} cm^{-3} for the 4-μm period sensor. From the observation of Fig. 5, it is clear that once the grating period is chosen from the sensing requirement, other parameters can be optimized to yield the best SPR condition. However, design parameters should be determined along with the limitation of practical fabrication protocols, which is discussed in Fig. 8.

As analytes selectively bind to the functionalized surface, the local refractive index of the analyte-binding layer changes, resulting in the change of the reflectance dip characteristics such as dip position, depth, and FWHM. Figure 6 shows the relative change of the reflectance dip position as a wavelength ($\Delta\lambda_{sp}$), the reflectance dip depth (ΔD_{sp}), and FWHM (ΔW_{sp}) as a function of the analyte-binding layer refractive index (n_f) for two different binding layer thicknesses (400 nm and 600 nm). As expected, when the refractive index of the analyte is the

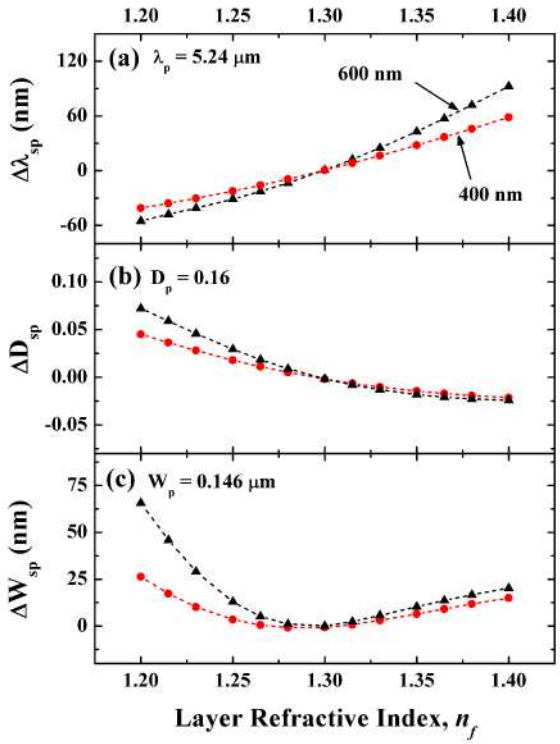

Fig. 6. Change in (a) position, (b) depth, and (c) FWHM of the reflectance dip with the refractive index change of 400-nm and 600-nm thick analyte-binding layers. For thicker samples, the dip geometries vary more drastically from the baseline point (n = 1.3). As the layer occupies a larger portion of the EM penetration depth, there is a substantial impact on the effective refractive index of the dielectric medium.

#130418 - $15.00 USD Received 24 Jun 2010; revised 7 Aug 2010; accepted 10 Aug 2010; published 27 Aug 2010

same as the background medium, i.e., n_{water} = 1.30 for water, there is no change in the SPR characteristics. Regardless of the sample thickness, the dip position, depth, and FWHM are all seen to asymmetrically change about the baseline layer refractive index. The resonance wavelength monotonically increases as the layer refractive index increases. The coupling strength between photons and surface plasmons, represented by reflectance dip depth, responds in an inverse manner, as it is shown in Fig. 6(b) to continually decrease as the layer's refractive index increases. The increase in FWHM in Fig. 6(c) suggest that the surface plasmon experiences radiation damping during its propagation mainly due to the increasing refractive index contrast between water and the analyte-binding layer [1,29]. This notion is demonstrated by a widening of the reflectance dip due to the presence of an analyte layer ($n_f \neq n_{water}$). For thicker samples, the dip geometries change more drastically, as the layer occupies a larger portion of the EM penetration depth and thus experiences substantial change on the effective refractive index of the water/sample combined dielectric medium.

In order to discuss the performance of the SPR sensor, Fig. 7 shows the detectable sample layer refractive index change as a function of the sample thickness when a Fourier transform infrared (FTIR) spectrometer is used to measure the reflectance spectrum with various spectral resolutions. Besides the tunability of the SPR, another advantage of the proposed SPR coupler is the easy integration with the FTIR spectrometry, which is readily accessible equipment in many laboratories. In order to examine the minimum detectable refractive index change of the analyte-binding layer, the reflectance dip positions for varying sample thicknesses and layer refractive indices were calculated and compared with the dip position when there is no analyte-binding layer. By correlating the dip position change $\Delta\lambda_{sp}$ with typical spectral resolutions of an FTIR spectrometer $\Delta\eta$, the detectable refractive index change of the analyte-binding layer $|\Delta n_f|$ at each layer thickness was estimated. That is, all areas above the dashed curves in the plot can be measured for any combination of refractive index and sample layer thickness.

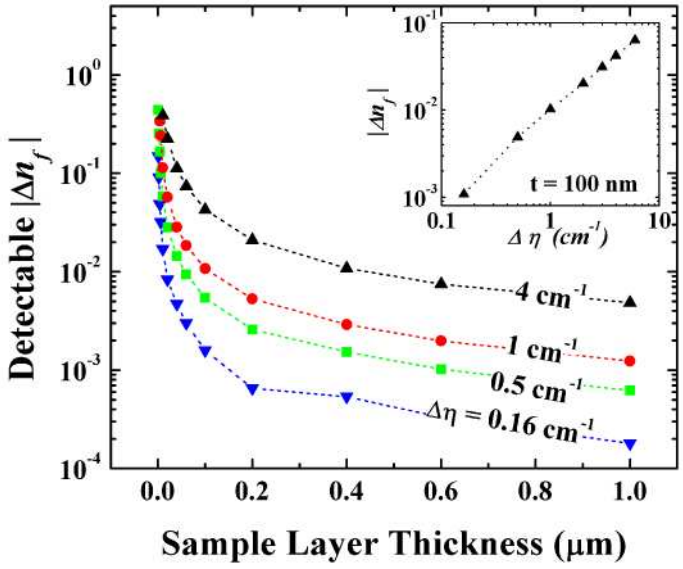

Fig. 7. Limit of detection determined by RCWA. The four curves plotted (0.16 cm^{-1}, 0.5 cm^{-1}, 1 cm^{-1} and 4 cm^{-1}) are typical spectral resolutions of an FTIR. All areas above the dashed curves in the plot can be measured for any combination of refractive index and sample layer thickness. Inset displays the detectable refractive index change of the analyte-binding layer as a function of the FTIR spectral resolution. Higher resolution settings will allow for the measurement of minute variations in surface composition.

#130418 - $15.00 USD Received 24 Jun 2010; revised 7 Aug 2010; accepted 10 Aug 2010; published 27 Aug 2010

The detection sensitivity of SPR sensors is defined as $S = \delta\lambda/\delta n_{ef}$ [7,10,13], where n_{ef} is the effective refractive index of a base medium and a thin analyte layer. When the layer thickness h is much thinner than the penetration depth of the SPP wave L_{pd}, as in our case, the effective refractive index change can be estimated as $\delta n_{ef} = 2h \cdot \delta n_f / L_{dp}$, where δn_f is the refractive index change of the analyte layer, under the assumption that the effective refractive index and the layer refractive index are the same as that of water at the surface plasmon wavelength [11]. From the inset of Fig. 7, the detection sensitivity of the SPR sensor at the layer thickness of t = 100 nm is estimated as 3022 nm/RIU. This sensitivity is much better than conventional metallic grating SPR sensors that has less than 750 nm/RIU in the visible and near-IR range [10]. The limit of detection (LOD) of the SPR sensor can be calculated from de Feijter formula [30], $\Delta\Gamma = h \cdot \delta n_{ef} / (dn/dc)_{vol}$, where $\Delta\Gamma$ is the surface concentration and $(dn/dc)_{vol}$ is the refractive index increment due to the analyte concentration change. Since $(dn/dc)_{vol}$ is a well-characterized property for most of the biochemical species and ranges typically from 0.1 to 0.3 cm^3/g [31], the limit of detectable surface concentration is estimated to be ~70 pg/mm^2 when the spectral resolution of 0.16 cm^{-1} and the analyte layer thickness of 100 nm are used for the estimation. This LOD is in fact one order of magnitude worse than the LOD of the current practical SPR biosensors, ~1 pg/mm^2 [32]. However, it should be noted that the estimated LOD of our SPR sensor is not the fundamental limit and is mainly limited by the spectral resolution of the FTIR spectrometer, the analyte layer thickness, and the SPR wavelength. The LOD thus can be improved by using a FTIR spectrometer capable of operating with a higher spectral resolution ($\Delta\eta < 0.16$ cm^{-1}). Also, mid-IR SPR excitation is not ideal for sample thicknesses used in the LOD analysis. The surface plasmon penetration depth (3.9 μm) is one order of magnitude larger than the 100 nm thin film; a smaller penetration depth provided by a shorter wavelength will considerably change the previously discussed effective refractive index when analyzing thin layers to improve the LOD.

Fabrication of the silicon coupler can be done using microelectromechanical system (MEMS) protocols. In order to achieve the targeted grating depth, four subsequent high-energy phosphorous implantations can be applied followed by the rapid thermal annealing for dopant activation. Previously performed RCWA calculations examined the ideal case of a uniform 10^{20} cm^{-3} phosphorous-impregnated trench, which immediately dropped to the concentration of the intrinsic silicon wafer (10^{14} cm^{-3}) at the end of the diffraction grating layer. However, as shown in the inset of Fig. 8, multiple doping and rapid annealing processes will create a non-uniform doping profile approximately 800 nm in depth, necessitating a more advanced RCWA analysis to confirm the excitation of surface plasmons in the fabricated structure. Up to 160 layers were added to the calculation with each layer having a unique depth dependent doping concentration. Another challenge in the sensor fabrication lies on the deposition of a sub-10 nm thick gold layer over a large sensing area. In order to improve the adhesion of the gold layer with Si, a thin Cr layer should be pre-deposited prior to the gold layer deposition. Thus, the effects of this adhesive layer on the SPR excitation also should be carefully examined. Figure 8 shows results for various possible combinations of practical MEMS processes in consideration. For the analysis, a 2-nm Cr layer was considered. The results shown in Fig. 7 indicate a comparable sharpness between the resonances achieved by the ideal case and actual grating profiles with direct Au (8 nm) deposition on Si and Cr (2 nm) + Au (6 nm) deposition. This result clearly demonstrates that surface plasmons can be excited with a fabricated SPR sensor. The real world obstacles of a multi-step ion implantation and a thin metal deposition layer will be overcome with carefully developing the processing recipe for each fabrication process, which remains as a future study.

#130418 - $15.00 USD Received 24 Jun 2010; revised 7 Aug 2010; accepted 10 Aug 2010; published 27 Aug 2010

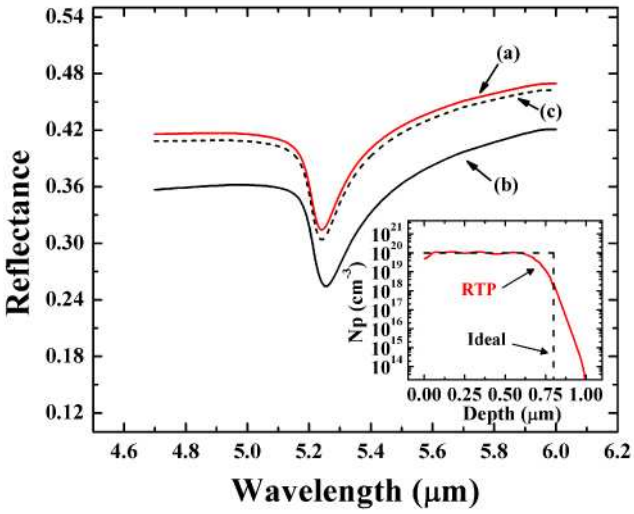

Fig. 8. Validation of surface plasmon excitation by the fabricated platform. Four phosphorous implants and the rapid thermal processing afterwards are required to produce a 800-nm deep grating structure, resulting in a non-uniform doping profile as shown in the inset. The RCWA calculation to account for the non-uniformity in doping concentration was completed for three different fabrication recipes: (a) a 8-nm gold layer deposited directly on the multi-step implanted Si grating, (b) a 2-nm Cr adhesion layer deposited prior to deposition of a 6-nm gold layer, and The calculation demonstrates that fabricated structures can excite a surface plasmon that is very similar to that of the ideal SPR platform, (c) a 8-nm gold layer deposited directly on the ideally doped Si grating.

4. Conclusion

This work presents a novel surface plasmon coupler that intends to resolve the problems at the moment impeding the advancement of conventional SPR based biosensors. A silicon diffraction grating curbs the intrinsic problems with current grating and prism-based couplers while maintaining their beneficial aspects. The silicon SPR grating coupler will also provide a peerless cost and adaptability while offering a competitive sensitivity with that of the high performance sensors currently in use today. The limit of detection for the doped-Si sensor was shown to be only one order of magnitude larger than current visible ranged SPR platforms even while analyzing layer thicknesses much smaller than the IR-SPR penetration depth. However, challenges arise during the fabrication of the proposed silicon biosensor. Achieving a uniform doping concentration while preventing unwanted lateral diffusions requires multiple ion implantations. Also, the exceedingly thin gold film required for the IR wave to evanescently tunnel through the metal layer pushes the limits of current MEMS metal deposition techniques. These challenges were overcome through the precise manipulation of the sensor's geometric parameters using RCWA to develop a fabrication protocol.

Acknowledgements

This work was supported by the URI startup program and the research development grant from the URI division of Research and Economic Development. We thank Prof. Z. Zhang and W. Euler for their valuable discussions.

#130418 - $15.00 USD Received 24 Jun 2010; revised 7 Aug 2010; accepted 10 Aug 2010; published 27 Aug 2010